Available online at www.sciencedirect.com
ScienceDirect
Journal of Power Sources 160 (2006) 1381–1386
JOURNAL OF POWER SOURCES
www.elsevier.com/locate/jpowsour

Structural, magnetic and electrochemical properties of lithium iron orthosilicate

K. Zaghib [a,*], A. Ait Salah [b], N. Ravet [c], A. Mauger [b], F. Gendron [b], C.M. Julien [b]

[a] *Institut de Recherche d'Hydro-Québec (IREQ), 1200 Boulevard Boulet, Varennes, Que., Canada J3X 1S1*
[b] *Institut des Nano-Sciences de Paris, UMR-CNRS 7588, Université Pierre et Marie Curie, 140 rue de Lourmel 75015 Paris, France*
[c] *Département de Chimie, Université de Montréal, Montréal, Que., Canada*

Received 1 February 2006; received in revised form 3 March 2006; accepted 6 March 2006
Available online 27 April 2006

Abstract

We report the structural and electronic characterization of Li_2FeSiO_4 synthesized by solid-state reaction. X-ray diffraction, Raman scattering, Fourier transform infrared (FTIR) spectroscopy, electron paramagnetic resonance (EPR) spectroscopy and magnetization measurements are analyzed. Magnetic susceptibility experiments give evidence that Li_2FeSiO_4 powders possess an antiferromagnetic ordering below $T_N = 25$ K due to long range Fe–O–Li–O–Fe interactions. Analysis of the paramagnetic region giving the Curie–Weiss parameters $\theta_p = -93.5$ K and $C_p = 4.13$ emu K mol^{-1} shows the divalent state of Fe cations. Electron paramagnetic resonance experiments confirm this electronic configuration. Electrochemical measurements were carried out in lithium cells with LiTFSI in a poly(ethylene oxide) (PEO) polymer electrolyte at 80 °C. The resulting cyclic voltammogram indicates a stable structure for the first cycle with redox peaks at 2.80 and 2.74 V versus Li^0/Li^+.

Keywords: Lithium batteries; Orthosilicate; Magnetic properties; Optical spectroscopy

1. Introduction

Since the demonstration of reversible lithium extraction/insertion in frameworks built with $(XO_4)^{n-}$ polyanions (X = P, S, As, Mo) there is pressure for further development of advanced positive electrodes for rechargeable Li-ion batteries [1]. In particular, $LiFePO_4$ with an ordered olivine structure has been extensively investigated [2–4]. The use of polyanions such as $(SiO_4)^{4-}$ in iron-based oxides could be advantageous because of the lower Fe^{3+}/Fe^{2+} redox. Orthosilicate Li_2MSiO_4 materials, where M is a divalent transition metal (M = Fe, Mn, Co), are compounds related to the Li_3PO_4 structure and are characterized by a tetrahedral coordination of all cations. Tarte and Cahay [5] have shown that members of the orthosilicate and orthogermanate groups have structures similar to the low-temperature form of Li_3PO_4. The structure of Li_3PO_4 has been accurately determined by Zemann who found that all cations (P and Li) are tetrahedrally coordinated [6]. Li_2MSiO_4 compounds have been reported to crystallize in the orthorhombic system with a $Pmn2_1$ space group. Fig. 1 displays the crystal structure of Li_2FeSiO_4 viewed along the *b*-axis. All the cations are tetrahedrally coordinated with oxygen atoms.

As far as the iron orthosilicate is concerned, there are a few reports on the physico-chemical properties of this material. The structural and magnetic properties of Li_2CoGeO_4 were investigated by Wintenberger [7]. An antiferromagnetic ordering was found below $T_N = 13.5$ K due to long range Co–O–Li–O–Co interactions. Recently, Li_2FeSiO_4 prepared by solid-state reaction has been proposed as a new positive electrode material for rechargeable Li-ion batteries [8].

In the present work, Li_2FeSiO_4 is synthesized by solid-state reaction and characterized by X-ray diffractometry (XRD), scanning electron microscopy (SEM), Raman scattering (RS), Fourier transform infrared (FTIR) spectroscopy, SQUID

* Corresponding author. Tel.: +1 450 652 8019; fax: +1 450652 8424.
E-mail address: karimz@ireq.ca (K. Zaghib).

0378-7753/$ – see front matter © 2006 Elsevier B.V. All rights reserved.
doi:10.1016/j.jpowsour.2006.03.023

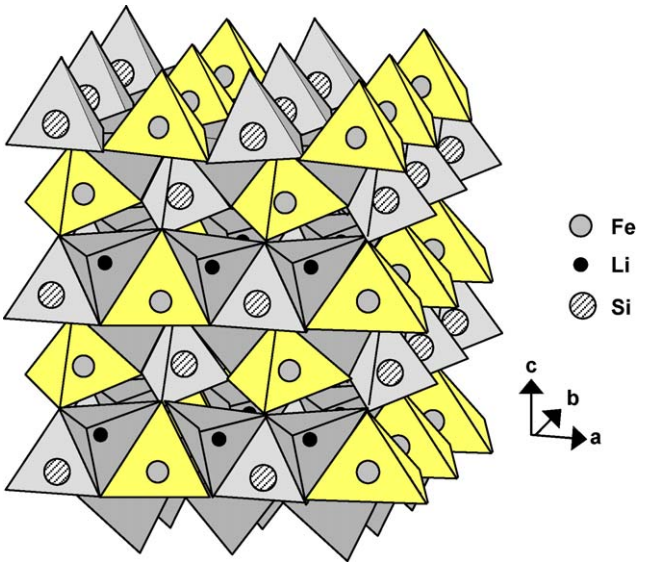

Fig. 1. The crystal structure of Li_2FeSiO_4 viewed along the *b*-axis. All the cations are tetrahedrally coordinated with oxygen atoms.

magnetometry and electron paramagnetic resonance (EPR). Detailed electrochemical studies involving cyclic voltammetry are reported.

2. Experimental

Powder samples of Li_2FeSiO_4 were synthesized by conventional solid-state reaction at moderate temperature. Stoichiometric Li_2SiO_3 with ferrous oxalate dehydrate $FeC_2O_4{\cdot}2H_2O$ (Fluka purum grade) were used as the starting materials. After a careful grinding for 6 h, the resulting mixture was transferred to a quartz ampoule in which some iron turnings were added. The ampoule was evacuated under secondary vacuum while kept at 200 °C and sealed. The reaction of $Li_2SiO_3 + FeC_2O_4{\cdot}2H_2O \rightarrow Li_2FeSiO_4$ was completed at 800 °C after 12 h. After cooling, the ampoule was opened under argon and the iron turnings were removed magnetically.

The X-ray diffractograms were recorded on a Philips X'Pert PRO MRD (PW3050) diffractometer equipped with a Cu anticathode (Cu Kα radiation $\lambda = 1.54056$ Å) at room temperature. The measurements have been recorded under Bragg–Brentano geometry at 2θ with step 0.05° in the range 10–80°. SEM observations were made by a high resolution electron microscope Hitachi (S-4700). The powders were sprinkled onto a adhesive carbon ribbon.

Fourier transform infrared absorption spectra were recorded using a Bruker IFS 113 vacuum interferometer. In the far infrared region (400–100 cm^{-1}), the vacuum bench apparatus was equipped with a 3.5 μm-thick Mylar beam splitter, a globar source and a DTGS/PE far-infrared detector. Raman spectra were measured using a Jobin-Yvon U1000 double pass spectrometer equipped with a cooled, low noise photomultiplier tube (ITT FW130). The incident light used for the experiments was the 515 nm Ar line of a laser source. The susceptibility and magnetization were measured using a superconducting quantum interference device (SQUID) magnetometer (Quantum Design MPMS). The data were recorded in both the zero-field cool (ZFC) and field cool (FC) mode with a magnetic field of $H = 0.5$ T. The derivative signals of the absorption spectra have been recorded with the use of a X-band VARIAN spectrometer. The powder samples have been placed in an ESR Oxford Instruments continuous flow cryostat, allowing measurements in the whole temperature range between room temperature and 3.5 K. The cryostat itself was inserted in a TE 102 microwave cavity. The frequency of the microwave field was 9.25 GHz. The frequency of the ac modulation magnetic field was 100 kHz, and the dc magnetic field varied in the range 0–2 T.

The electrochemical properties of the product were investigated at 80 °C in two-electrode cells with metallic lithium as the negative electrode using Teflon laboratory-cell hardware and a Mac-Pile system. The electrochemical investigations were made in lithium batteries with poly(ethylene oxide) (PEO) bis-trifluoromethanesulfnonimide salt (LiTFSI) as electrolyte with a ratio O/Li of 20. Composite cathodes were made of the electroactive material, acetylene black, PEO in the proportion 33, 10, 57 (% weight), acetonitrile was added to dissolve the PEO. These components were intimately mixed together and spread on a carbon coated aluminium current collector. Cyclic voltammograms were carried out versus Li^0/Li^+ at slow scan rate 20 mV h^{-1}.

3. Results and discussion

3.1. Structure and morphology

Fig. 2 shows the XRD diagram of the orthosilicate Li_2FeSiO_4 crystalline powders. The X-ray diffraction data for the Li_2FeSiO_4 phase may be indexed to the orthorhombic unit cell in space group $Pmn2_1$ typical of phases with the low-temperature Li_3PO_4 structure type [9]. Four intense diffraction peaks are recorded at $d = 5.345$, 3.358, 2.703 and 2.510 Å corresponding to the (0 1 0), (2 0 0), (0 0 2) and (0 2 1) lines, respectively. The lattice constants have been calculated to be $a = 6.263$, $b = 5.331$ and $c = 5.015$ Å. These values are consistent with those reported previously [5,8].

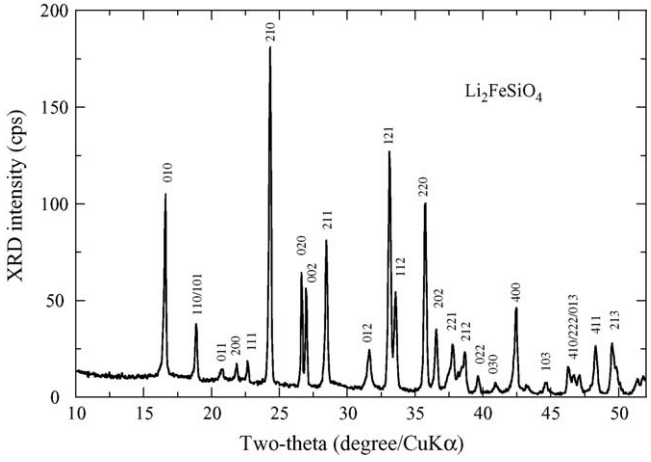

Fig. 2. X-ray diffraction pattern of Li_2FeSiO_4 crystalline powders.

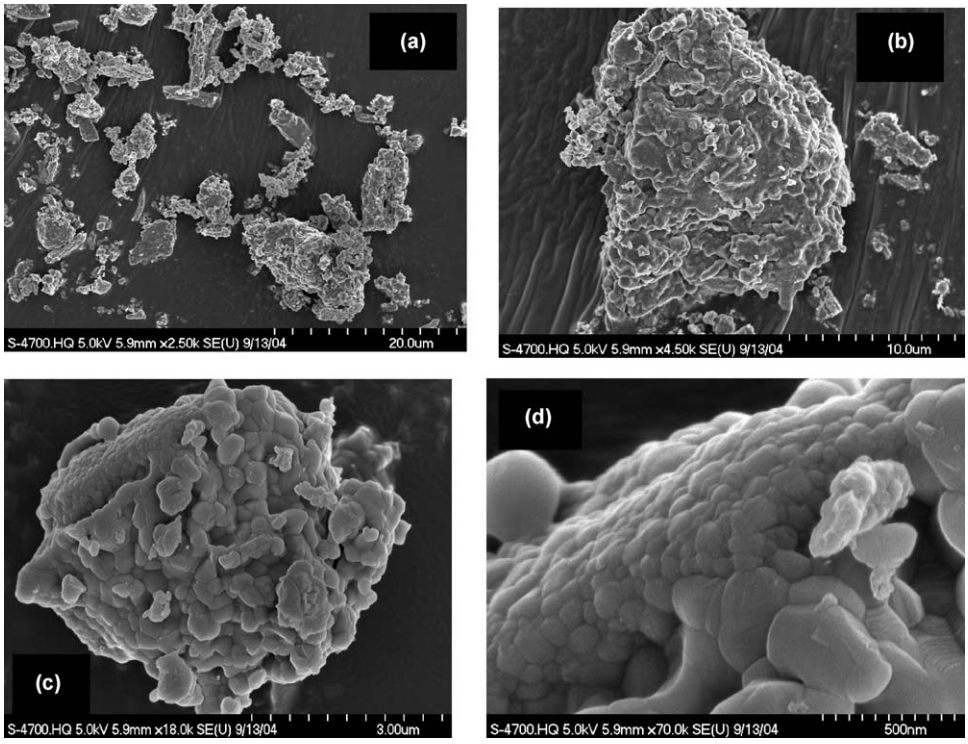

Fig. 3. SEM image of Li_2FeSiO_4 powders synthesized by solid-state reaction.

The degree of crystallinity of the Li_2FeSiO_4 powders, i.e. particle shape, crystallite size, domain size, was examined by XRD and SEM. At first, the crystallite size, δ, is estimated from the XRD pattern with the aid of the Scherrer's formula

$$\delta = 0.9\frac{\lambda}{B\cos\theta}, \quad (1)$$

where λ is the X-ray wavelength ($\lambda = 1.5406$ Å) and B is the FWHM of the XRD peak in radians. The average crystallite size of powders grown by solid-state reaction is found to be 78 nm.

The shape and morphology of the particles in orthosilicate samples were followed by SEM observations. Fig. 3a–d presents the SEM images with various magnifications of the products calcined at 750 °C. It is shown that the Li_2FeSiO_4 powders consist of well-developed particles. The remarkable spherical shape of the particles is attributed to the careful synthesis of the product including extensive grinding between successive calcinations. The average particle size for materials prepared by solid-state reaction at 750 °C (Fig. 3d) is estimated to be 80–100 nm that is in agreement with XRD data. Moreover, the Li_2FeSiO_4 powders exhibit a uniform particle size distribution.

3.2. Lattice dynamics

Vibrational properties of silicate-based materials can be treated by assuming the separation of the vibrations into internal modes of SiO_4 units and external modes. Lattice dynamics of silicate-based compounds was made using the correlation method of Fateley et al. [10]. The results for Li_2FeSiO_4 crystal ($Pmn2_1$–C_{2v}^7 space group) are shown in Table 1. Vibrational modes of tetrahedral SiO_4 molecules are well known [11]. In order to facilitate the analysis of the vibrational spectra, we performed a factor group analysis for the internal and external vibrations of the SiO_4 groups in the orthosilicate lattice, correlating the point group of the "free" ion (T_d) with its site group (C_s^{xz}) and the factor group (C_{2v}). Internal modes involve the displacement of oxygen atoms of the tetrahedral $(SiO_4)^{4-}$ anions and present frequencies closely related to those of the free

Table 1
Factor group analysis for the orthosilicate structure, $Pmn2_1$ space group (C_{2v}^7) in which (R) and (IR) represent Raman- and infrared-active vibrations, respectively

Translations of Li, Ni and Si atoms		
Atom	Site group	Factor group C_{2v}
Li	C_1	$A_1 + A_2 + 2B_1 + 2B_2$
Fe	C_1	$A_1 + A_2 + 2B_1 + 2B_2$
Si	C_s^{xz}	$2A_1 + 2B_1 + A_2 + B_2$
Internal modes of SiO_4		
Point group T_d	Site group C_s^{xz}	Factor group C_{2v}
A_1	A'	$A_1 + B_1$
E	$A' + A''$	$A_1 + B_1 + A_2 + B_2$
F_2	$2A' + A''$	$2A_1 + 2B_1 + A_2 + B_2$
F_2	$2A' + A''$	$2A_1 + 2B_1 + A_2 + B_2$
Librations of SiO_4		
Point group T_d	Site group C_s^{xz}	Factor group C_{2v}
F_1	$A' + 2A''$	$A_1 + B_1 + 2B_2 + 2A_2$
Total amount of allowed optical modes	$\Gamma = 10A_1(R,IR) + 8A_2(R) + 12B_1(R,IR) + 9B_2(R,IR)$	

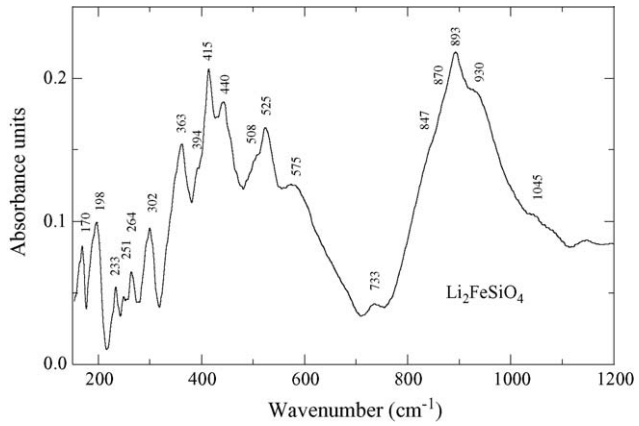

Fig. 4. FTIR spectrum of Li_2FeSiO_4 crystalline powders.

molecule. For $(SiO_4)^{4-}$, these are a singlet (A_1) at a frequency $\nu_1 = 819\,cm^{-1}$; a doublet (E) at $\nu_2 = 340\,cm^{-1}$ and two triply degenerate (F_2) modes, ν_3 at $956\,cm^{-1}$ and ν_4 at $527\,cm^{-1}$. ν_1 and ν_3 involve the symmetric and asymmetric stretching mode of the Si–O bonds, whereas ν_2 and ν_4 involve mainly O–Si–O symmetric and asymmetric bending mode with a small contribution of Si vibration [12]. In a solid, internal modes can split as a consequence of two effects: the site-symmetry effect due to an electric crystal field of symmetry lower than tetrahedral acting on the molecule and the correlation effect due to the presence of more than one molecular group in the crystal unit cell.

Figs. 4 and 5 present the FTIR and Raman scattering spectra of Li_2FeSiO_4 crystalline powders, respectively. As the structure of orthosilicate is built from LiO_4 and FeO_4 tetrahedra linked to $(SiO_4)^{4-}$ polyanions, the local cationic arrangement can be discussed with the aid of factor group analysis and molecular vibration model [12]. The internal (SiO_4) vibrations of Li_2FeSiO_4 can be derived from the fundamental $(SiO_4)^{4-}$ modes ν_1–ν_4, and that the stretching and bending mode regions are well separated from each other. As expected, the vibrational spectra are dominated by the fundamental vibrations of the $(SiO_4)^{4-}$ polyanions which are split in many components due to the correlation effect induced by the coupling with of Fe–O and Li–O tetrahedral units in the structure.

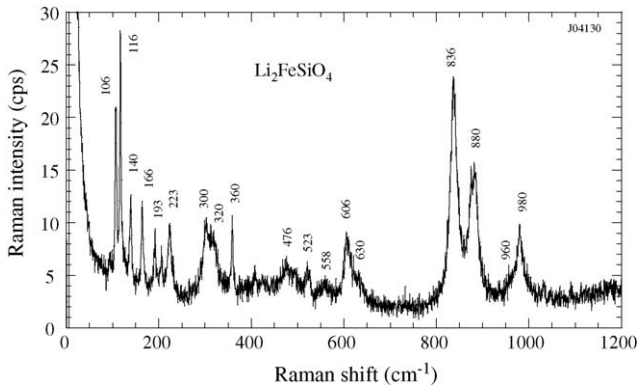

Fig. 5. Raman scattering spectrum of Li_2FeSiO_4 crystalline powders.

In the infrared region of the internal modes of the silicate anion (1000–800 cm^{-1} region), we can identify the asymmetric stretching (ν_1) mode at $847\,cm^{-1}$ and the triplet (ν_3) modes at 870, 893 and $930\,cm^{-1}$. The corresponding modes for the orthosilicate Zn_2SiO_4 have been pointed at 872, 905, 934 and $978\,cm^{-1}$ [12]. The bending (ν_4) IR-active modes of $(SiO_4)^{4-}$ oxo-anions are located at 510–575 cm^{-1}. The RS and FTIR spectra display the mutual activity of the weak band at ca. $730\,cm^{-1}$ which is attributed to the vibration of O–Si–O bridging bonds. A remarkable aspect of the Raman spectrum is the well-resolved low-frequency region, i.e. domain of the lattice modes that confirms the good crystallinity of the sample. As expected, the Li_2FeSiO_4 crystalline phase has a four-peak RS spectrum in the high-wavenumber region where internal modes of the silicate anion appear. The Raman features of unequal intensities appear at 836, 880, 960 and $980\,cm^{-1}$ that are the symmetric stretching Raman-active modes. The peak at $836\,cm^{-1}$ is the totally symmetric ($A_1 + B_1$) mode and the bands at 880, 960 and $980\,cm^{-1}$ are attributed to the ($A_1 + B_1 + A_2 + B_2$) components. The medium wavenumber peaks at 630, 606, 558 and 523 are originating from the degenerate bending ν_4 mode.

However, the Li_2FeSiO_4 phase cannot be considered as a molecular solid even if the tetrahedral $(SiO_4)^{4-}$ oxo-anions have strong covalent bonding. Orthosilicate materials have been indicated to have vibrations intermediate between well-defined internal modes (e.g. $CaCO_3$) and purely lattice mode (e.g. MgO) [12]. Although, the treatment of the medium-frequency vibrational modes of Li_2FeSiO_4 does not work in terms of a molecular model. In addition to the features so far assigned to the SiO_4 molecular unit, there are also features in the RS and FTIR spectra due to tetrahedrally coordinated Li^+ and Fe^{2+} cations that require additional discussion. The difficulty comes from the mixture of the FeO_4, LiO_4 and SiO_4 related modes appearing at frequency below $600\,cm^{-1}$. Nevertheless, the IR bands involving the stretching motion of LiO_4 tetrahedral units have been recorded at 348–534 cm^{-1} in the isomorphic structure Li_3PO_4 [13]. These vibrations appear at 363–440 for Li_2FeSiO_4 while vibrations involving the motion FeO_4 tetrahedra occurs at wavenumbers 300–360 cm^{-1}.

3.3. Electronic properties

Magnetic experiments are powerful tools to study fundamental properties and to check the quality of samples [14]. The magnetic quantities, i.e. magnetic moment $M(H,T)$ and molar susceptibility $\chi_m(T)$, obtained from SQUID magnetometry give evidence of the electronic properties of the Li_2FeSiO_4 orthosilicate powders. However, it is necessary to correlate the magnetic susceptibility $\chi_m(T)$ curves and isothermal $M(H)$ plots for a complete analysis of the electronic properties of materials. Fig. 6 shows the temperature dependence of the inverse molar magnetic susceptibility χ_m of Li_2FeSiO_4 powders for field cooled (open circles) and zero-field cooled (full circles) experiments. Here, χ_m is defined as the ratio M/H with M the magnetization measured in the applied field ($H = 5$ kG). The arrow point out the anomalies characteristics of an antiferromagnetic ordering of Li_2FeSiO_4 below $T_N = 25$ K. The most outstanding property of

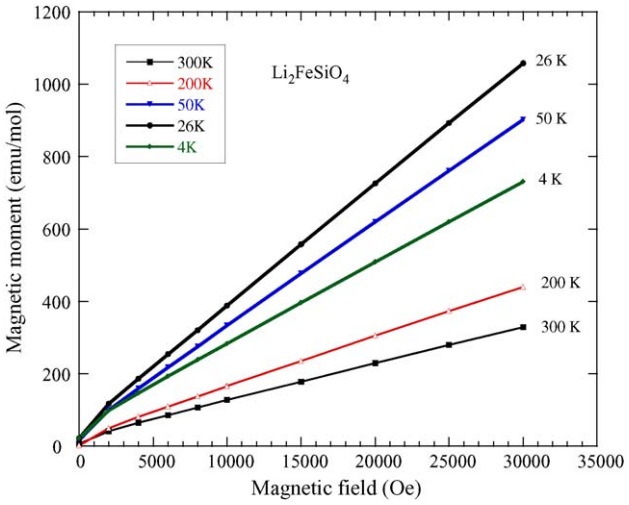

Fig. 6. Temperature dependence of the inverse molar magnetic susceptibility χ_m of Li_2FeSiO_4 powders for field cooled (open circles) and zero-field cooled (full circles) experiments. χ_m defined as the ratio M/H with M the magnetization measured in the applied field ($H = 5$ kG). The arrow point out the anomalies characteristics of antiferromagnetic ordering of Li_2FeSiO_4 at $T_N = 25$ K.

the $\chi_m^{-1}(T)$ curve for Li_2FeSiO_4 lies in the fact that the deviation from the Curie–Weiss law remains small in the paramagnetic region above 80 K.

Fig. 7 shows the magnetization curve $M(H)$ for Li_2FeSiO_4 crystalline powders as a function of the temperature in the range 4–300 K. Clearly, the curves M/H are a linear function of the magnetic field for $H > 5$ kG. The small curvature of the plots $M(H)$ at low magnetic field indicates that some ferromagnetic or ferrimagnetic component is present in the Li_2FeSiO_4 framework. The magnetic susceptibility $\chi_m = dM/dH$ calculated from the isothermal magnetization data is plotted in Fig. 8. Analysis of susceptibility data $\chi_m(T)$ in the high temperature range shows the paramagnetic regime according the Curie–Weiss' law

$$\chi_m = \frac{N_A p_{eff}^2 \mu_B^2}{3k_B} \frac{1}{T + \theta_p}, \quad (2)$$

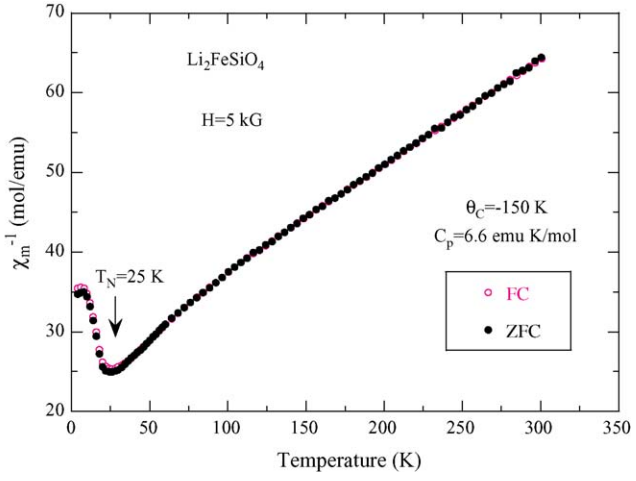

Fig. 7. Magnetization curve $M(H)$ as a function of the temperature for Li_2FeSiO_4 crystalline powders.

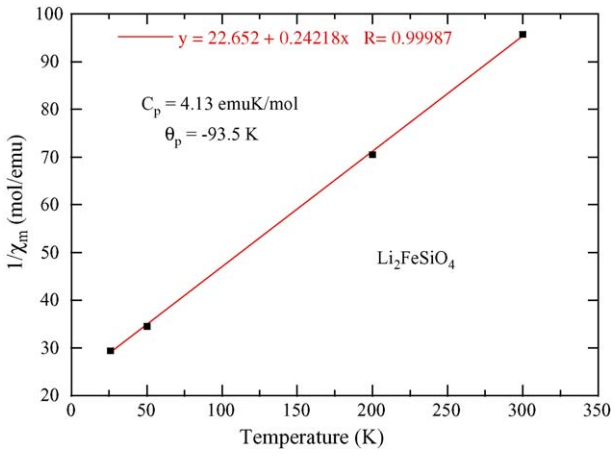

Fig. 8. Plot of the temperature dependence of the reciprocal magnetic susceptibility obtained from the slope dM/dH of the magnetization curves for Li_2FeSiO_4 crystalline powders.

where the first fraction is the Curie constant C_p, N_A is the Avogadro number, k_B the Boltzamn constant, p_{eff} the effective magnetic moment, μ_B the Bohr magneton and θ_p is the Weiss constant. From the fitting of the curve $\chi_m^{-1}(T)$, one obtains the value $C_p = 4.13$ emu K mol^{-1} and $\theta_p = -93.5$ K. Our magnetization measurements show the development of a paramagnetic moment approaching $\mu_{eff} = 5.68\mu_B$, consistent with the spin-only of Fe^{2+} ions in the configuration of a strong cubic crystal field. The negative value of θ_p is consistent with the antiferromagnetic coupling for this compound. The magnetic data are consistent with a stoichiometric sample, supporting the results from the XRD and FTIR data. However, the magnetic ground state of Li_2FeSiO_4 is very sensitive to various crystal imperfections and readily changes to a weak ferromagnetic state upon synthesis conditions.

Fig. 9 presents the temperature dependence of the EPR spectra for Li_2FeSiO_2 crystalline powders. The EPR signal is very weak in the studied sample. At the frequency used in the experiments, such a signal is centered at $H = 3000$ G. Let us recall that

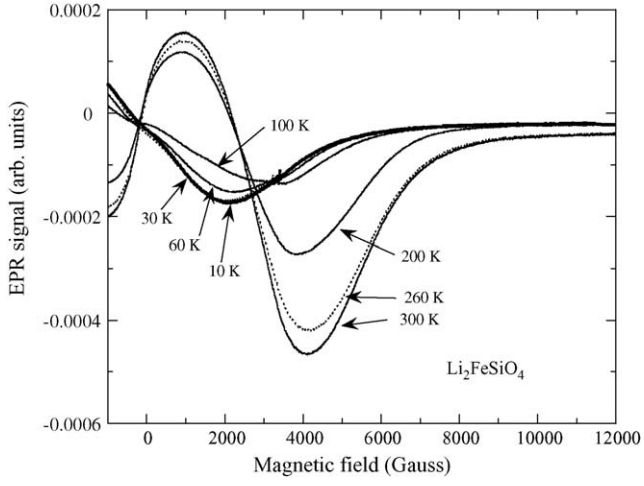

Fig. 9. Temperature dependence of the EPR spectra for Li_2FeSiO_2 crystalline powders.

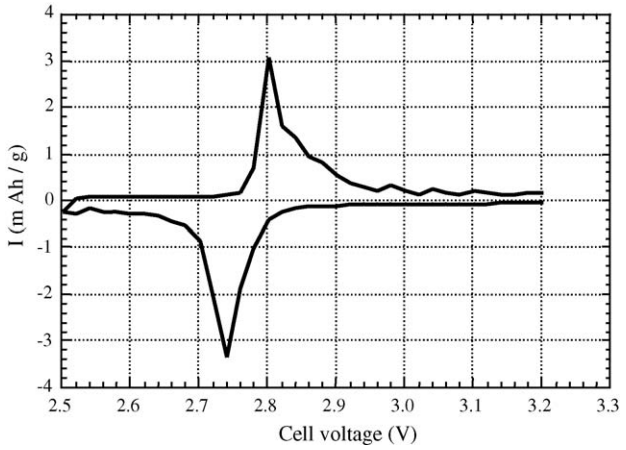

Fig. 10. Slow scan cyclic voltammetry (20 mV h^{-1}) obtained at 80 °C with a Li/POE-LiTFSI/Li_2FeSiO_4 battery.

no EPR signal should be detected in absence of magnetic defects or impurity features due to the configuration of the Fe^{2+} ($3d^6$) ions. This very weak signal is the signature of uncoupled spins in such a small concentration that it may be due to any residual impurities or defects such as an unpaired electron spin associated to an oxygen vacancy or to a defect such as an Fe^{3+} ion associated to a lithium vacancy. This kind of defect is very sensitive to its local neighborhood, which can explained the large broadening of the EPR line.

3.4. Electrochemical properties

Fig. 10 presents the cyclic voltammogram recorded at slow scan 20 mV h^{-1} of the Li//Li_2FeSiO_4 electrochemical cell. In this electrochemical cell configuration, we are using the molten-salt LiTFSI-based in polymer (PEO) electrolyte at an operating temperature of 80 °C. Results shown in Fig. 10 demonstrate that the charge–discharge process occurs with the appearance of a single phase. We looked for any appearance of sharp peak that could be the fingerprint of a voltage plateau for a two-phase system or the occurrence of some phase transformation. The oxido-reduction process is totally reversible. The oxidation and reduction reactions appear at ca. 2.80 and 2.74 V versus Li^0/Li^+, respectively. This cell does not display the phase transition during the first experimental cycling runaway that has been reported by Nyten et al. [8] in their "impure" Li_2FeSiO_4. The absence of the extra oxidation peak at 3.1 V is attributed to the high quality of the Li_2FeSiO_4 electrode material for which purity has been previously checked by magnetic measurements.

4. Conclusion

Crystallo-chemical studies of the orthosilicate Li_2FeSiO_2 have shown that this compound crystallizes in the orthorhombic structure ($Pmn2_1$ space group). Characterizations of the structure and morphology of powders have been performed using XRD, SEM, Raman, FTIR, while electronic properties of materials have been investigated by SQUID magnetometry and EPR spectroscopy. The Li_2FeSiO_2 sample synthesized from a solid-state reaction exhibits well-formed crystallites of 80–100 nm in size. Vibrational spectra show that the Li_2FeSiO_2 material can be treated as a molecular compound for the internal vibrational modes of $(SiO_4)^{4-}$ oxo-anions but factor group analysis is required for vibrations involving motions of Li–O and Fe–O bonds in the tetrahedral units. The magnetic properties of Li_2FeSiO_2 show an antiferromagnetic ordering below $T_N = 25$ K. The magnetic ground state of Li_2FeSiO_2 is very sensitive to various crystal imperfections and readily changes to a weak ferromagnetic state upon synthesis. Electrochemical measurements carried out in lithium cells with LiTFSI in a PEO polymer electrolyte at 80 °C, show single phase behavior without any transformation after the first cycle. The resulting cyclic voltammogram indicates a stable structure for the first cycle with redox peaks at 2.80 and 2.74 V versus Li^0/Li^+.

References

[1] A.K. Padhi, K.S. Nanjundaswamy, J.B. Goodenough, J. Electrochem. Soc. 144 (1997) 1188.
[2] A. Yamada, S.C. Chung, K. Hinikuma, J. Electrochem. Soc. 148 (2001) A229.
[3] K. Zaghib, J. Shim, A. Guerfi, P. Charest, K.A. Striebel, Electrochem. Solid-State Lett. 8 (2005) A207.
[4] H. Huang, S.-C. Yin, L.F. Nazar, Electrochem. Solid-State Lett. 4 (2001) A170.
[5] P. Tarte, R. Cahay, C.R. Acad. Sc. Paris C271 (1970) 777.
[6] J. Zemann, Acta Crystallogr. 13 (1960) 863.
[7] M. Wintenberger, C.R. Acad. Sc. Paris C271 (1970) 669.
[8] A. Nyten, A. Abouimrane, M. Armand, T. Gustafsson, J.O. Thomas, Electrochem. Commun. 7 (2005) 156.
[9] C. Keffer, A. Mighell, F. Mauer, H. Swanson, S. Block, Inorg. Chem. 6 (1967) 119.
[10] W.F. Fateley, F.R. Dollish, N.T. McDevitt, F.F. Bentley, Infrared and Raman Selection Rules for Molecular and Lattice Vibrations: The Correlation Method, Wiley–Interscience, New York, 1972.
[11] K. Nakamoto, Infrared and Raman Spectra of Inorganic and Coordination Compounds, Wiley & Sons, New York, 1978.
[12] P. Tarte, Spectrochim. Acta 18 (1962) 467.
[13] P. Tarte, Spectrochim. Acta 29 (1967) 915.
[14] A. Ait Salah, K. Zaghib, A. Mauger, F. Gendron, C.M. Julien, Phys. Status Solidi (a) 203 (2006) R1.